Journal of Systems Engineering and Electronics
Vol. 32, No. 4, August 2021, pp.956 – 970

Stability analysis of linear/nonlinear switching active disturbance rejection control based MIMO continuous systems

WAN Hui[1], QI Xiaohui[1], and LI Jie[2,*]

1. Department of Unmanned Aerial Vehicle Engineering, Army Engineering University of PLA, Shijiazhuang 050003, China;
2. The 32nd Research Institute, China Electronics Technology Group Corporation, Shanghai 201800, China

Abstract: In this paper, a linear/nonlinear switching active disturbance rejection control (SADRC) based decoupling control approach is proposed to deal with some difficult control problems in a class of multi-input multi-output (MIMO) systems such as multi-variables, disturbances, and coupling, etc. Firstly, the structure and parameter tuning method of SADRC is introduced into this paper. Followed on this, virtual control variables are adopted into the MIMO systems, making the systems decoupled. Then the SADRC controller is designed for every subsystem. After this, a stability analyzed method via the Lyapunov function is proposed for the whole system. Finally, some simulations are presented to demonstrate the anti-disturbance and robustness of SADRC, and results show SADRC has a potential applications in engineering practice.

Keywords: linear/nonlinear switching active disturbance rejection control (SADRC), multi-input multi-output (MIMO) continuous system, decoupling control, stability analysis.

DOI: 10.23919/JSEE.2021.000082

1. Introduction

After proposing the tracking differentiator (TD) [1,2], non-linear state error feedback (NLSEF) [3] and the extended state observer (ESO) [4], Han formally advanced active disturbance rejection control (ADRC) in 1998 [5]. ADRC is an unconventional control technique as it is a significant difference from both modern and classical control theories. It reflects Han's unique understanding about the control theory, such as "model analysis approach or a direct control approach" [6], "linear and nonlinear of feedback system" [7], and so on. On the one hand, it takes advantage of the proportional-integral-derivative (PID) control law which is almost model free. On the other hand, inspired by the state observer technique of modern control, this theory combines both the internal and external disturbances as well as uncertainties of the plant as "total disturbance " and uses an ESO to estimate and compensate it. It is a big breakthrough of "time invariant and time varying" and "linear and nonlinear", since the time-varying part and the nonlinear part of the system can be considered as uncertainty. For this reason, ADRC has got increasing attention and a wide range of engineering applications in recent years.

The original ADRC proposed by Han contains nonlinear functions and is mentioned as nonlinear ADRC (NLADRC) in this study. The nonlinear structures of NLADRC make it difficult to perform theoretical research and a retarded period is observed during the preliminary development of ADRC. However, some inspiring results about convergence and stabilization have been achieved recently, laying a good foundation for theoretical studies of NLADRC. For example, the convergence of the NLADRC based closed-loop system is proved for a class of single-input single-output (SISO) systems [8], multi-input multi-put (MIMO) systems [9] and lower triangular systems with uncertainty [10]. Meanwhile, stabilization works are mainly around the limit cycle analysis, absolute stability and Lyapunov's stability. The limit cycle analysis of the ESO including one or two nonlinearities is established via the describing function method [11−13]. In some recent published works [14–17], the absolute stability for the nominal satisfying constraint of norm growth is studied separately. Moreover, the local asymptotic stability for the NLADRC based closed-loop system containing multi-nonlinearities is also derived [18].

In 2003, Gao linearized the ADRC, which was called ADRC (LADRC) [19], facilitating the theoretical studies and applications with a splendid advancement of this

Manuscript received November 10, 2020.
*Corresponding author.
This work was supported by the Scientific Research Innovation Development Foundation of Army Engineering University ((2019)71).

field. Up to now, the ADRC has successfully been applied in many products [20] and a large number of researches on convergence and stabilization have been achieved. Yoo et al. [21] and Yang et al. [22] proved that the estimate error of the linear ESO (LESO) is bounded on the condition that the "total disturbance" is bounded or its derivative is bounded. The works of Shao et al. [23], Yoo et al. [24] and Huang et al. [25] quantitatively discussed the convergence of the discrete-time LESO. Based on the works of Zheng et al. [26] and Chen et al. [27], the estimation ability of the LESO and the stability of the closed-loop LADRC based system are demonstrated with and without the plant model. Xue and Huang [28] proved the stability of LADRC for a class of SISO systems (linear or nonlinear, time-varying or time-invariant) with unknown dynamics and disturbance. While Xue et al. [29] proposed an LADRC controller for a class of MIMO block lower-triangular systems and analyzed the dynamic and steady performance of the closed-loop. Moreover, the performance analysis of ADRC for nonlinear uncertain systems with unknown dynamics and discontinuous disturbances is reported before as well [30].

Though researchers prefer LADRC due to its simple parameter tuning, clear physical meaning and easy theoretical analysis characteristics, NLADRC is potentially much more effective in tolerance to uncertainties, disturbance and improvement of system dynamics. To combine the advantages of both systems and make NLADRC easier for application, we accomplish the following work: analyzing the stability of NLADRC based nominal continuous systems [13,14,18] and plants with parameter perturbation or disturbance satisfying constraint of norm growth [15], laying a foundation of improving system stability and optimizing control ability; proposing general principles and simple formulas for the parameter tuning of nonlinear ESO (NLESO) and applying them to general cases [31]; quantitatively studying the advantages and disadvantages of LADRC and NLADRC, and proposing a new control approach, called linear nonlinear switching ADRC (SADRC) [31,32], providing a new pathway for the development of ADRC. Controller design and stability analysis of the SADRC based on the SISO system is also achieved and corresponding simulations also verify the effectiveness in anti-disturbance and tracking accuracy.

Previous work only focused on the SISO systems, while further investigation should be carried out in MIMO systems which are common in industry and much more challenging due to the multi-variables, multi-disturbances and interactions. Therefore, this paper designs the SADRC based decoupling control approach for a class of MIMO continuous systems and proposes a stability analysis method based on the Lyapunov function which is easy to understand and use in practice via computer calculation.

This paper is structured as follows: Section 2 describes the principle and framework of SADRC, then designs the SADRC based controller for a class of MIMO systems, followed by the stability analysis. Two cases are studied to validate the effectiveness of the proposal by simulations in Section 3. Finally, some conclusions are given in Section 4.

2. Control design and stability analysis

2.1 Framework and algorithm of SADRC

The SADRC aims to combine the advantages of both LADRC and NLADRC. Therefore, we first take a class of SISO continuous systems as an example to illustrate the structure of NLADRC, LADRC and the principle of SADRC.

ADRC generally consists of TD, ESO and state error feedback (SEF). TD is mainly used to extract the derivatives of the reference signal and relatively independent in controller design. ESO is used to estimate the system states and the total disturbance, which is the core and essence of the ADRC. SEF is used to restrain the residual error and achieve the desired control goal. For the sake of facilitating the stability analysis, TD is exempted in the controller design, and we only introduce the structure of ESO and SEF here.

2.1.1 Structure of NLADRC/LADRC

Consider a class of n-dimensional SISO continuous systems described by

$$\begin{cases} \dot{x}_1 = x_2 \\ \dot{x}_2 = \dot{x}_3 \\ \quad\vdots \\ \dot{x}_n = f(x_1, x_1, \cdots, x_n, w, t) + bu \\ y = x_1 \end{cases} \tag{1}$$

where $x_1, \cdots, x_n$ are the system states, $f(x_1, x_2, \cdots, x_n, w, t)$ denotes the "total disturbance", w represents external disturbances, y and u are the output and input of the system, respectively, and b is a constant control coefficient. The objective of NLADRC, LADRC or SADRC is to design a controller to make the output y track a reference input v_1, and x_i track v_i $(i = 2, \cdots, n)$ provided that the latter exists in some sense.

For the above plant, take $x_{n+1} = f(x, \dot{x}, \cdots, x_n, w, t)$ as the extended state of system (1), then the ESO of system (1) is designed as follows:

$$\begin{cases} e = z_1 - y \\ \dot{z}_1 = z_2 - \beta_{01}\varphi_1(e) \\ \quad \vdots \\ \dot{z}_n = z_{n+1} - \beta_{0n}\varphi_n(e) + b_0 u \\ \dot{z}_{n+1} = -\beta_{0(n+1)}\varphi_{(n+1)}(e) \end{cases} \tag{2}$$

where $z_i(i = 1,2,\cdots,n)$ is the observed value which provides an estimation of the system state and z_{n+1} provides an estimation of the "total disturbance"; $\beta_{0i}(i = 1,2,\cdots,n+1)$ is the observer gain.

If $\varphi_i(e)(i = 1,2,\cdots,n+1)$ is a nonlinear function, (2) is called the NLESO, a common form of $\varphi_i(e)(i = 1,2,\cdots,n+1)$ is defined as

$$\varphi_i(e) = \text{fal}(e,\alpha_i,\delta) = \begin{cases} \dfrac{e}{\delta^{\alpha_i - 1}}, & |e| \leqslant \delta \\ |e|^{\alpha_i}\text{sign}(e), & |e| > \delta \end{cases} \tag{3}$$

where δ represents the range of the linearity of $\varphi_i(e)(i = 1,2,\cdots,n+1)$ which should be pre-determined according to the practical applications; $\alpha_i(i = 1, 2, \cdots, n+1)$ is constant when α_i $(i = 1, 2, \cdots, n+1)$ is constants, $\varphi_i(e)(i = 1,2,\cdots,n+1)$ has characteristics of relative small error, big gain, big error, small gain, while when α_i=1$(i = 1, 2, \cdots, n + 1)$, nonlinear function $\varphi_i(e)$ $(i = 1,2,\cdots,n+1)$ turns to be linear and (2) is called LESO.

The nonlinear SEF (NLSEF) of system (1) is designed [31] as

$$\begin{cases} u_0 = \sum_{i=1}^{n} k_i \text{fal}_i(v_i - z_i, \alpha'_i, \delta'_i) \\ u = (u_0 - z_{n+1})/b \end{cases}. \tag{4}$$

A linear one can be described as

$$\begin{cases} u_0 = \sum_{i=1}^{n} k_i(v_i - z_i) \\ u = (u_0 - z_{n+1})/b \end{cases}. \tag{5}$$

If the ESO and the SEF are both linear, the designed controller is called LADRC, otherwise, NLADRC.

2.1.2 SADRC principle

As the key component of ADRC, ESO is used to estimate and eliminate the model uncertainties and elucidate the influence of external disturbances on the system. It turns out that the accuracy of ESO directly affects the control performance. Therefore, in this paper, the linear SEF (LSEF) is chosen here while SADRC represents the switch between LESO and NLESO based on state error, a scheme of SADRC is given as follows:

(i) If there are possible initial state errors between the states of the plant and the ESO, NLESO is adopted during a transition time T (artificially set) to avoid "peaking phenomenon"; otherwise, this step is skipped and the system directly goes into the following step;

(ii) After step (i), the controller automatically switches between LESO and NLESO according to the error e. Choose a specific δ_s, when $e < \delta_s$, NLESO starts to work; otherwise, LESO begins to work. δ_s is a general boundary of the performance of LESO and NLESO, i.e., when $e < \delta_s$, NLESO is superior to LESO, whereas LESO is superior to NLESO. δ_s can be determined by simulation, experiment or theoretical computation [31].

The above process is also shown in Fig.1. In general, this scheme of SADRC unites the merits of LADRC and NLADRC.

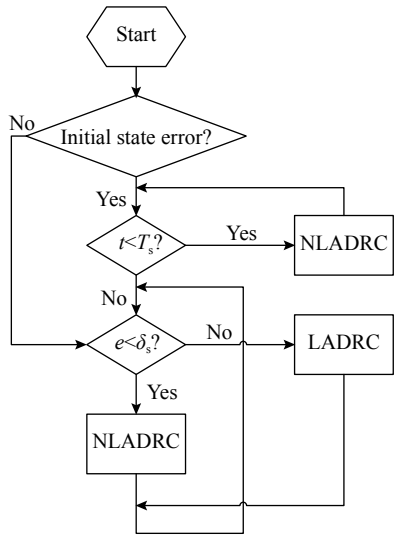

Fig. 1 Scheme of SADRC

The structure of SADRC will be discussed in detail with the controller design of SADRC based MIMO continuous system in the next section.

2.1.3 MIMO continuous systems

In this paper, we consider a class of MIMO continuous systems composed of coupled subsystems with external disturbances described by

$$\begin{cases} \mathrm{d}\boldsymbol{x}_i(t) = \boldsymbol{A}_{s_i}\boldsymbol{x}_i(t)\mathrm{d}t + \boldsymbol{B}_{s_i}\left[f_i(t,\boldsymbol{x}(t),w_i(t)) + \sum_{l=1}^{m} c_{il}u_l(t)\right]\mathrm{d}t \\ \boldsymbol{y}_i(t) = \boldsymbol{C}_{s_i}\boldsymbol{x}_i(t) \end{cases} \tag{6}$$

where $i = 1,2,\cdots,m$, $\boldsymbol{x}(t) = (\boldsymbol{x}_1{}^{\mathrm{T}}(t),\cdots,\boldsymbol{x}_m{}^{\mathrm{T}}(t))^{\mathrm{T}} \in \mathbf{R}^{n\times m}(g_1 = g_2 = \cdots = g_m = n)$, $\boldsymbol{u}(t) = (u_1(t),\cdots,u_m(t))^{\mathrm{T}} \in \mathbf{R}^m$, $\boldsymbol{y}(t) = (\boldsymbol{y}_1{}^{\mathrm{T}}(t),\cdots,\boldsymbol{y}_m{}^{\mathrm{T}}(t))^{\mathrm{T}} \in \mathbf{R}^{n\times m}$ represents the state, the control input and the output of the system (6), respectively; $g_1 = g_2 = \cdots = g_m = n$ means that every subsystem of sys-

tem (6) is n-dimensional; $f_i(t,\boldsymbol{x}(t),w_i(t))$ denotes the "total disturbance" of the subsystem $\boldsymbol{x}_i(t)$, and $w_i(t)$ represents the corresponding external disturbance; $c_{il}(i,l=1,2,\cdots,m)$ is the control coefficient.

$\boldsymbol{A}_{s_i}=\begin{pmatrix}0 & \boldsymbol{I}_{g_i-1}\\ 0 & 0\end{pmatrix}_{g_i\times g_i}$, $\boldsymbol{B}_{s_i}=(0,\cdots,0,1)^{\mathrm{T}}_{g_i\times 1}$, $\boldsymbol{C}_{s_i}=(1,\cdots,0,0)^{\mathrm{T}}_{1\times g_i}$

Then the control gain matrix $\boldsymbol{C}$ is described as

$$\boldsymbol{C}=\begin{pmatrix}c_{11} & c_{12} & \cdots & c_{1m}\\ c_{21} & c_{22} & \cdots & c_{2m}\\ \vdots & \vdots & \ddots & \vdots\\ c_{m1} & c_{m2} & \cdots & c_{mm}\end{pmatrix}. \tag{7}$$

Suppose matrix $\boldsymbol{C}$ is invertible or generalized inverse matrices exist, and define virtual control input as $\boldsymbol{u}_{\mathrm{v}}(t)=(u_{1\mathrm{v}}(t),u_{2\mathrm{v}}(t),\cdots,u_{m\mathrm{v}}(t))^{\mathrm{T}}\in\mathbf{R}^m$, system (6) can be rewritten as

$$\begin{cases}\mathrm{d}\boldsymbol{x}_i(t)=\boldsymbol{A}_{s_i}\boldsymbol{x}_i(t)\mathrm{d}t+\boldsymbol{B}_{s_i}\left[f_i(t,\boldsymbol{x}(t),w(t))+u_{i\mathrm{v}}(t)\right]\mathrm{d}t\\ \boldsymbol{y}_i(t)=\boldsymbol{C}_{s_i}\boldsymbol{x}_i(t)\end{cases} \tag{8}$$

where $i=1,2,\cdots,m$, $\boldsymbol{u}_{\mathrm{v}}(t)=\boldsymbol{C}\boldsymbol{u}(t)$.

For the subsequent stability analysis, define the following vector $\boldsymbol{x}_{\mathrm{s}}(t)=(\boldsymbol{x}_{\mathrm{s}1}{}^{\mathrm{T}}(t),\cdots,\boldsymbol{x}_{sn}{}^{\mathrm{T}}(t))^{\mathrm{T}}\in\mathbf{R}^{m\times n}(h_1=h_2=\cdots=h_n=m)$, where $x_{si}(t)=(x_{si1}(t),\cdots,x_{sm}(t))^{\mathrm{T}}\in\mathbf{R}^m$ represents the same order states of subsystems, then the system (8) can be rewritten as

$$\begin{cases}\mathrm{d}\boldsymbol{x}_{\mathrm{s}}(t)=\boldsymbol{A}\boldsymbol{x}_{\mathrm{s}}(t)\mathrm{d}t+\boldsymbol{B}[\boldsymbol{u}_{\mathrm{v}}(t)+f(t,\boldsymbol{x}(t),w(t))]\mathrm{d}t\\ \boldsymbol{y}(t)=\boldsymbol{x}_{\mathrm{s}1}(t)\end{cases} \tag{9}$$

where

$$\boldsymbol{A}=\begin{bmatrix}\boldsymbol{0} & \boldsymbol{I} & \boldsymbol{0} & \boldsymbol{0} & \boldsymbol{0}\\ \boldsymbol{0} & \boldsymbol{0} & \boldsymbol{I} & \boldsymbol{0} & \boldsymbol{0}\\ \vdots & \vdots & \ddots & \vdots & \vdots\\ \boldsymbol{0} & \boldsymbol{0} & \boldsymbol{0} & \boldsymbol{I} & \boldsymbol{0}\\ \boldsymbol{0} & \boldsymbol{0} & \boldsymbol{0} & \boldsymbol{0} & \boldsymbol{0}\end{bmatrix}\in\mathbf{R}^{mn\times mn},\boldsymbol{B}=\begin{bmatrix}\boldsymbol{0}\\ \boldsymbol{I}\end{bmatrix}\in\mathbf{R}^{mn\times m},$$

$$\boldsymbol{I}=\begin{bmatrix}1 & 0 & 0 & 0\\ 0 & 1 & 0 & 0\\ \vdots & \vdots & \ddots & \vdots\\ 0 & 0 & 0 & 1\end{bmatrix}\in\mathbf{R}^{m\times m},\quad f(t,\boldsymbol{x}(t),w(t))=(f_1(t,\boldsymbol{x}(t),$$

$w(t)),f_2(t,\boldsymbol{x}(t),w(t)),\cdots,f_m(t,\boldsymbol{x}(t),w(t)))^{\mathrm{T}}$.

2.1.4 Structure of SADRC

Take one of the subsystems as an example, the SESO is designed as follows:

$$\begin{cases}e_i=z_{i1}-y_i\\ \dot{z}_{i1}=z_{i2}-\beta_{i01}\mathrm{fs}_{i1}(e_i)\\ \quad\vdots\\ \dot{z}_{is_i}=z_{i(s_i+1)}-\beta_{i0s_i}\mathrm{fs}_{is_i}(e_i)+u_{iv}\\ \dot{z}_{i(s_i+1)}=-\beta_{i0(s_i+1)}\mathrm{fs}_{i(s_i+1)}(e_i)\end{cases} \tag{10}$$

where z_{ij} (i =1, 2, ⋯, m; j = 1, 2, ⋯, s_i+1) is the estimation of x_{ij} (i =1, 2, ⋯, m; j = 1, 2, ⋯, s_i+1) in x-subsystem, and $z_{i(s_i+1)}$ is the estimation of "total disturbance", s_i=n; β_{i0j} (i =1, 2, ⋯, m; j = 1, 2, ⋯, s_i+1) is the NLESO's gain in SESO, and suppose β_{i0jL} (i =1, 2, ⋯, m; j = 1, 2, ⋯, s_i+1) the LESO's gain in SESO, is λ_{ij} (i =1, 2, ⋯, m; j = 1, 2, ⋯, s_i+1) multiple of the NLESO' gain, λ_{ij} is constant. Then the switching function $\mathrm{fs}_{ij}(e)$ (i =1, 2, ⋯, m; j = 1, 2, ⋯, s_i+1) can be described as

$$\mathrm{fs}_{ij}(e_i)=\begin{cases}\mathrm{fL}_{ij}(e_i), & |e_i|\leqslant\delta_{is}\\ \lambda_{ij}e_i, & |e|>\delta_{is}\end{cases} \tag{11}$$

where δ_{is} is the critical value for the switching between NLESO and LES; $\mathrm{fL}_{ij}(e_i)$ (i =1, 2, ⋯, m; j = 1, 2, ⋯, s_i + 1) is the nonlinear function of NLESO, defined as

$$\mathrm{fL}_{ij}(e_i)=\mathrm{fal}(e_i,\alpha_{ij},\delta_i)=\begin{cases}\dfrac{e_i}{\delta_i^{\alpha_{ij}-1}}, & |e_i|\leqslant\delta_i\\ |e_i|^{\alpha_{ij}}\mathrm{sign}(e_i), & |e_i|>\delta_i\end{cases} \tag{12}$$

where $\alpha_{ij}<1$.

For the subsequent stability analysis, define

$$\frac{\mathrm{fL}_{ij}(e_i)}{e_i}\cdot e_i=\varsigma_{0ij}(e_i)e_i. \tag{13}$$

Let

$$\lambda_{0ij}(e_i)=\begin{cases}\varsigma_{0ij}(e_i), & |e_i|\leqslant\delta_{is}\\ \lambda_{ij}, & |e_i|>\delta_{is}\end{cases}. \tag{14}$$

The SESO (10) can be rewritten as

$$\begin{cases}e_i=z_{i1}-y_i\\ \dot{z}_{i1}=z_{i2}-\beta_{i01}\cdot\lambda_{0i1}(e_i)\cdot e_i\\ \quad\vdots\\ \dot{z}_{is_i}=z_{i(s_i+1)}-\beta_{i0s_i}\cdot\lambda_{0is_i}(e_i)\cdot e_i+u_{iv}\\ \dot{z}_{i(s_i+1)}=-\beta_{i0(s_i+1)}\cdot\lambda_{0i(s_i+1)}(e_i)\cdot e_i\end{cases} \tag{15}$$

where $i=1,2,\cdots,m$; $s_i=n$.

The LESF of SADRC can be described as

$$\begin{cases}u_{iv0}=\sum_{q=1}^{n}k_{iq}\cdot(v_{iq}-z_{iq})\\ u_{iv}=u_{iv0}-z_{i(s_i+1)}\end{cases} \tag{16}$$

where v_{iq} (q = 1,2,⋯,n) is the reference input; k_{iq}(q = 1,2,⋯,n) is the controller gain.

2.1.5 Decoupling controller design based on SADRC

Consider the engineering application, make the following assumptions for the MIMO systems.

Assumption 1 The reference inputs and their all-order derivatives are assumed to be bounded.

Assumption 2 The changing rate of disturbances are assumed to be bounded.

Defining the desired values of every state: $\boldsymbol{x}_{\mathrm{d}}(t)=(\boldsymbol{x}_{1\mathrm{d}}{}^{\mathrm{T}}(t),\cdots,\boldsymbol{x}_{n\mathrm{d}}{}^{\mathrm{T}}(t))^{\mathrm{T}}\in\mathbf{R}^{m\times n}(h_1=h_2=\cdots=h_n=m)$, error

vector: $\boldsymbol{\delta}(t)=(\boldsymbol{\delta}_1{}^{\mathrm{T}}(t),\cdots,\boldsymbol{\delta}_n{}^{\mathrm{T}}(t))^{\mathrm{T}}\in R^{m\times n}(r_1=r_2=\cdots=r_n=m)$, where $\boldsymbol{\delta}_i(t)=(\boldsymbol{x}_{i1}(t)-\boldsymbol{x}_{di1}(t),\cdots,\boldsymbol{x}_{im}(t)-\boldsymbol{x}_{dim}(t))\in\mathbf{R}^m$, substitute $\boldsymbol{x}_{\mathrm{d}}(t)$ and $\boldsymbol{\delta}(t)$ into (9), then we obtain

$$\mathrm{d}\boldsymbol{\delta}(t)=\boldsymbol{A}\boldsymbol{\delta}(t)\mathrm{d}t+\boldsymbol{B}[\boldsymbol{u}_{\mathrm{v}}(t)+f(t,\boldsymbol{x}(t),w(t))-\dot{\boldsymbol{x}}_{\mathrm{nd}}^{\mathrm{T}}(t)]\mathrm{d}t. \tag{17}$$

Then the objective of the controller will find LESF to make $\boldsymbol{\delta}(t)$ converge asymptotically to zero.

SESO is used to estimate the "total disturbance" of the system, take $f(t,\boldsymbol{x}(t),w(t))$ as the extended state of system (9), define $\boldsymbol{\varsigma}(t)=(\boldsymbol{\varsigma}_1{}^{\mathrm{T}}(t),\cdots,\boldsymbol{\varsigma}_n{}^{\mathrm{T}}(t),\boldsymbol{\varsigma}_{n+1}{}^{\mathrm{T}}(t))^{\mathrm{T}}=(\boldsymbol{x}_{\mathrm{s}1}{}^{\mathrm{T}}(t),\cdots,\boldsymbol{x}_{sn}{}^{\mathrm{T}}(t),f(t,\boldsymbol{x}(t),w(t)))^{\mathrm{T}}$ then the state-space model of system (9) with the extended state can be described as

$$\begin{cases}\mathrm{d}\boldsymbol{\varsigma}(t)=\boldsymbol{A}_0\boldsymbol{\varsigma}(t)\mathrm{d}t+[\boldsymbol{B}_0\boldsymbol{u}_{\mathrm{v}}(t)+\boldsymbol{E}_0\boldsymbol{h}(t)]\,\mathrm{d}t\\ \boldsymbol{y}(t)=\boldsymbol{\varsigma}_1(t)\end{cases} \tag{18}$$

where $\boldsymbol{h}(t)=\dot{f}(t,\boldsymbol{x}(t),w(t))$, and assume $\boldsymbol{h}(t)$ is bounded;

$$\boldsymbol{A}_0=\begin{bmatrix}\boldsymbol{0}&\boldsymbol{I}&\boldsymbol{0}&\boldsymbol{0}\\ \boldsymbol{0}&\boldsymbol{0}&\boldsymbol{I}&\boldsymbol{0}\\ \vdots&\vdots&\ddots&\vdots\\ \boldsymbol{0}&\boldsymbol{0}&\boldsymbol{0}&\boldsymbol{I}\\ \boldsymbol{0}&\boldsymbol{0}&\boldsymbol{0}&\boldsymbol{0}\end{bmatrix}\in\mathbf{R}^{m(n+1)\times m(n+1)},\quad \boldsymbol{B}_0=\begin{bmatrix}\boldsymbol{0}\\ \boldsymbol{I}\\ \boldsymbol{0}\end{bmatrix}\in$$

$\mathbf{R}^{m(n+1)\times m}$, $\boldsymbol{E}_0=\begin{bmatrix}\boldsymbol{0}\\ \boldsymbol{0}\\ \boldsymbol{I}\end{bmatrix}\in\mathbf{R}^{m(n+1)\times m}$.

The SESO for system (18) can be designed as

$$\mathrm{d}\hat{\boldsymbol{\varsigma}}(t)=\boldsymbol{A}_0\hat{\boldsymbol{\varsigma}}(t)\mathrm{d}t+[\boldsymbol{B}_0\boldsymbol{u}_v(t)+\boldsymbol{L}\boldsymbol{Q}(\boldsymbol{\varsigma}(t)-\hat{\boldsymbol{\varsigma}}(t))]\,\mathrm{d}t \tag{19}$$

where $\hat{\boldsymbol{\varsigma}}(t)=(\hat{\boldsymbol{\varsigma}}_1^{\mathrm{T}}(t),\cdots,\hat{\boldsymbol{\varsigma}}_n^{\mathrm{T}}(t),\hat{\boldsymbol{\varsigma}}_{n+1}^{\mathrm{T}}(t))^{\mathrm{T}}$ is the estimation of $\boldsymbol{\varsigma}(t)$, and $\hat{\boldsymbol{\varsigma}}_{n+1}^{\mathrm{T}}(t)$ is the estimation of the "total disturbance"; and $\boldsymbol{L}$ is the observer gain vector.

$$\boldsymbol{L}=\begin{bmatrix}\boldsymbol{\alpha}_{c1}&\cdots&\boldsymbol{\alpha}_{cn}&\boldsymbol{\alpha}_{c(n+1)}\end{bmatrix}^{\mathrm{T}}\in\mathbf{R}^{m(n+1)\times m},$$

$$\boldsymbol{\alpha}_{cg}=\mathrm{diag}(\boldsymbol{\alpha}_{cg1},\cdots,\boldsymbol{\alpha}_{cgm})=$$

$$\mathrm{diag}(\beta_{10g}\cdot\lambda_{01g},\cdots,\beta_{m0g}\cdot\lambda_{0mg}),\ g=1,2,\cdots,n+1,$$

$$\boldsymbol{Q}=\begin{bmatrix}\boldsymbol{I}&\boldsymbol{0}&\boldsymbol{0}\end{bmatrix}\in\mathbf{R}^{m\times m(n+1)}$$

The LESF of the system is defined as

$$\begin{cases}\boldsymbol{u}_{\mathrm{v}}(t)=-\boldsymbol{K}\boldsymbol{\delta}(t)+\boldsymbol{x}_{\mathrm{nd}}{}^{\mathrm{T}}(t)-\hat{f}(t,\boldsymbol{x}(t),w(t))\\ \hat{f}(t,\boldsymbol{x}(t),w(t))=\hat{\boldsymbol{\varsigma}}_{n+1}^{\mathrm{T}}(t)\end{cases} \tag{20}$$

where $\boldsymbol{K}=\begin{bmatrix}\boldsymbol{K}_1,\boldsymbol{K}_2,\cdots,\boldsymbol{K}_n\end{bmatrix}$, and $\boldsymbol{K}_g=\mathrm{diag}(k_{g1},\cdots,k_{gm})$ $(g=1,2,\cdots,n)$ is the control gain; $\hat{f}(t,x(t),w(t))$ is the estimation of $f(t,x(t),w(t))$.

Substituting (20) into (19), we have

$$\mathrm{d}\boldsymbol{\delta}(t)=\boldsymbol{A}_{\mathrm{H}}\boldsymbol{\delta}(t)\mathrm{d}t+\boldsymbol{B}[f(t,\boldsymbol{x}(t),w(t))-\hat{f}(t,\boldsymbol{x}(t),w(t))]\mathrm{d}t \tag{21}$$

where $\boldsymbol{A}_{\mathrm{H}}=\boldsymbol{A}-\boldsymbol{B}\boldsymbol{K}$. If parameters of $\boldsymbol{K}$ are chosen to make $\boldsymbol{A}_{\mathrm{H}}$ Hurwitz, system (21) is globally asymptotically stable.

2.2 Stability analysis

Define observer error vector $\tilde{\boldsymbol{\varsigma}}(t)=\boldsymbol{\varsigma}(t)-\hat{\boldsymbol{\varsigma}}(t)$.

Let

$$\boldsymbol{M}(t)=(\boldsymbol{M}_1{}^{\mathrm{T}}(t),\cdots,\boldsymbol{M}_n{}^{\mathrm{T}}(t),\boldsymbol{M}_{n+1}{}^{\mathrm{T}}(t))^{\mathrm{T}} \tag{22}$$

where $\boldsymbol{M}_i(t)=\tilde{\boldsymbol{\varsigma}}_i(t)(i=1,\cdots,n+1)$.

Combining (18), (19) and (21), we obtain

$$\mathrm{d}\boldsymbol{M}(t)=(\boldsymbol{A}_0-\boldsymbol{L}\boldsymbol{Q})\boldsymbol{M}(t)\mathrm{d}t+\boldsymbol{E}_0\boldsymbol{h}(t)\mathrm{d}t. \tag{23}$$

Then the LESF of (20) can be rewritten as

$$\begin{cases}\boldsymbol{u}_{\mathrm{v}}(t)=-\boldsymbol{K}\boldsymbol{\delta}(t)+\begin{bmatrix}\boldsymbol{K}&\boldsymbol{0}_{m\times m}\end{bmatrix}\tilde{\boldsymbol{\varsigma}}(t)+\\ \qquad\dot{\boldsymbol{x}}_{\mathrm{nd}}^{\mathrm{T}}(t)-\hat{\boldsymbol{\varsigma}}_{n+1}^{\mathrm{T}}(t)\\ \hat{f}(t,\boldsymbol{x}(t),w(t))=\hat{\boldsymbol{\varsigma}}_{n+1}^{\mathrm{T}}(t)\end{cases}. \tag{24}$$

Substituting (24) into (17), we get

$$\mathrm{d}\boldsymbol{\delta}(t)=\boldsymbol{A}_{\mathrm{H}}\boldsymbol{\delta}(t)\mathrm{d}t+\begin{bmatrix}\boldsymbol{B}\boldsymbol{K}&\boldsymbol{B}\end{bmatrix}\tilde{\boldsymbol{\varsigma}}(t)\mathrm{d}t. \tag{25}$$

Combining (23) and (25), we have

$$\begin{cases}\mathrm{d}\boldsymbol{\delta}(t)=\boldsymbol{A}_{\mathrm{H}}\boldsymbol{\delta}(t)\mathrm{d}t+\begin{bmatrix}\boldsymbol{B}\boldsymbol{K}&\boldsymbol{B}\end{bmatrix}\tilde{\boldsymbol{\varsigma}}(t)\mathrm{d}t\\ \mathrm{d}\boldsymbol{M}(t)=(\boldsymbol{A}_0-\boldsymbol{L}\boldsymbol{Q})\boldsymbol{M}(t)\mathrm{d}t+\boldsymbol{E}_0\boldsymbol{h}(t)\mathrm{d}t\end{cases}. \tag{26}$$

2.2.1 Observer error system stability analysis

Theorem 1 Consider the observer error dynamics of (21) under Assumption 2, if the observer gain vector $\boldsymbol{L}$ is chosen such that $(\boldsymbol{A}_0-\boldsymbol{L}\boldsymbol{Q})$ is stable, then $\boldsymbol{M}(t)$ exponentially converges to the bounded ball $\boldsymbol{B}_{r1}=\boldsymbol{M}(t)\in\mathbf{R}^{m(n+1)\times1}$, $\|\tilde{\boldsymbol{\varsigma}}(t)\|\leqslant2\lambda_{\max}(\boldsymbol{P}_0)\boldsymbol{h}_{\max}$, where $\lambda_{\max}(\boldsymbol{P}_0)$ is the maximum eigenvalue of $\boldsymbol{P}_0$, $\boldsymbol{P}_0$ is the solution of the equation $(\boldsymbol{A}_0-\boldsymbol{L}\boldsymbol{Q})^{\mathrm{T}}\boldsymbol{P}_0+\boldsymbol{P}_0(\boldsymbol{A}_0-\boldsymbol{L}\boldsymbol{Q})=-\boldsymbol{I}_{m(n+1)\times m(n+1)}$, and $\boldsymbol{h}_{\max}$ is the absolute maximum value of $\boldsymbol{h}(t)$ [33].

Proof Define the Lyapunov function V as follows:

$$V(t)=\boldsymbol{M}(t)^{\mathrm{T}}\boldsymbol{P}_0\boldsymbol{M}(t). \tag{27}$$

Taking the derivative of V, we get

$$\begin{aligned}\dot{V}(t)=\boldsymbol{M}(t)^{\mathrm{T}}\left[(\boldsymbol{A}_0-\boldsymbol{L}\boldsymbol{Q})^{\mathrm{T}}\boldsymbol{P}_0+\boldsymbol{P}_0(\boldsymbol{A}_0-\boldsymbol{L}\boldsymbol{Q})\right]\boldsymbol{M}(t)+\\ 2\boldsymbol{M}(t)^{\mathrm{T}}\boldsymbol{P}_0\boldsymbol{E}_0\boldsymbol{h}(t)\leqslant-\|\boldsymbol{M}(t)\|^2+\\ 2\|\boldsymbol{M}(t)\|\|\boldsymbol{P}_0\|\boldsymbol{h}_{\max}\leqslant-\|\boldsymbol{M}(t)\|[\|\boldsymbol{M}(t)\|-2\lambda_{\max}(\boldsymbol{P}_0)\boldsymbol{h}_{\max}].\end{aligned} \tag{28}$$

Thus $\dot{V}(t)<0$, whenever $\|\boldsymbol{M}(t)\|>2\lambda_{\max}(\boldsymbol{P}_0)\boldsymbol{h}_{\max}$. $\boldsymbol{M}(t)$ exponentially converges to bounded ball $\boldsymbol{B}_{r1}=\boldsymbol{M}(t)\in\mathbf{R}^{m(n+1)\times1}$, $\|\tilde{\boldsymbol{\varsigma}}(t\|\leqslant2\lambda_{\max}(\boldsymbol{P}_0)\boldsymbol{h}_{\max}$.

Remark 1 From (19), we can conclude that, if $\boldsymbol{Q}$ converges to zero, $\tilde{\boldsymbol{\varsigma}}$ will converge to zero, thus $\hat{\boldsymbol{\varsigma}}\to\boldsymbol{\varsigma}$.

2.2.2 Closed-loop system stability analysis

Consider the closed-loop system (26). Define $\boldsymbol{\delta}_{\rm cl}(t)=[\boldsymbol{\delta}(t),\boldsymbol{M}(t)]^{\rm T}$, the the system (26) can be rewritten as

$$\mathrm{d}\boldsymbol{\delta}_{\rm cl}(t)=\boldsymbol{A}_{\rm cl}\boldsymbol{\delta}_{\rm cl}(t)\mathrm{d}t+\boldsymbol{B}_{\rm cl}\boldsymbol{h}(t)\mathrm{d}t \tag{29}$$

where $\boldsymbol{A}_{\rm cl}=\begin{bmatrix}\boldsymbol{A}_{\rm H} & \begin{bmatrix}\boldsymbol{BK} & \boldsymbol{B}\end{bmatrix}\\ \boldsymbol{0} & \boldsymbol{A}_0-\boldsymbol{LQ}\end{bmatrix},\boldsymbol{B}_{\rm cl}=\begin{bmatrix}\boldsymbol{0}\\ \boldsymbol{E}_0\end{bmatrix}$.

Theorem 2 Consider the closed-loop system (27) under Assumption 2, if the gain vector $\boldsymbol{K}$ and the observer gain vector $\boldsymbol{L}$ are chosen such that $\boldsymbol{A}_{cl}$ is Hurwitz, then $\boldsymbol{\delta}_{\rm cl}(t)$ exponentially converges to the bounded ball $\boldsymbol{B}_{r2}=\boldsymbol{\delta}_{\rm cl}(t)\in\mathbf{R}^{(mn+m(n+1))\times 1}$, $\|\boldsymbol{\delta}_{\rm cl}(t)\|\leqslant 2\lambda_{\max}(\boldsymbol{P}_{cl})\boldsymbol{h}_{\max}$, where $\lambda_{\max}(\boldsymbol{P}_{\rm cl})$ is the maximum eigenvalue of $\boldsymbol{P}_{\rm cl}$, $\boldsymbol{P}_{\rm cl}$ is the solution of equation $\boldsymbol{A}_{\rm cl}{}^{\rm T}\boldsymbol{P}_{\rm cl}+\boldsymbol{P}_{\rm cl}\boldsymbol{A}_{\rm cl}=-\boldsymbol{I}_{(mn+m(n+1))\times(mn+m(n+1))}$, $\boldsymbol{h}_{\max}$ is the absolute maximum value of $\boldsymbol{h}(t)$.

Proof Define the Lyapunov function V_1 as follows:

$$V_1(t)=\boldsymbol{\delta}_{\rm cl}(t)^{\rm T}\boldsymbol{P}_{\rm cl}\boldsymbol{\delta}_{\rm cl}(t). \tag{30}$$

Taking the derivative of $V_1(t)$, we obtain

$$\begin{aligned}\dot{V}_1(t)=&\boldsymbol{\delta}_{\rm cl}(t)^{\rm T}\left[\boldsymbol{A}_{\rm cl}{}^{\rm T}\boldsymbol{P}_{\rm cl}+\boldsymbol{P}_{\rm cl}\boldsymbol{A}_{\rm cl}\right]\boldsymbol{\delta}_{\rm cl}(t)+\\ &2\boldsymbol{\delta}_{\rm cl}(t)^{\rm T}\boldsymbol{P}_{\rm cl}\boldsymbol{B}_{\rm cl}\boldsymbol{h}(t)\leqslant\\ &-\|\boldsymbol{\delta}_{\rm cl}(t)\|^2+2\|\boldsymbol{\delta}_{\rm cl}(t)\|\|\boldsymbol{P}_{\rm cl}\|\boldsymbol{h}_{\max}\leqslant\\ &-\|\boldsymbol{\delta}_{\rm cl}(t)\|(\|\boldsymbol{\delta}_{\rm cl}(t)\|-2\lambda_{\max}(\boldsymbol{P}_{\rm cl})\boldsymbol{h}_{\max}).\end{aligned} \tag{31}$$

Thus $\dot{V}_1(t)<0$ whenever $\|\boldsymbol{\delta}_{\rm cl}(t)\|>2\lambda_{\max}(\boldsymbol{P}_{\rm cl})\boldsymbol{h}_{\max}$. $\boldsymbol{\delta}_{\rm cl}(t)$ exponentially converges to the bounded ball $\boldsymbol{B}_{r2}=\boldsymbol{\delta}_{\rm cl}(t)\in\mathbf{R}^{(mn+m(n+1))\times 1}$, $\|\boldsymbol{\delta}_{\rm cl}(t)\|\leqslant 2\lambda_{\max}(\boldsymbol{P}_{\rm cl})\boldsymbol{h}_{\max}$. □

3. Case study

In this section, two case studies are used to test the anti-disturbance and robustness of SADRC, LADRC, and NLADRC. For a fair comparison, the parameters of most controllers are transported from the public literatures.

3.1 Binary distillation column system

3.1.1 Binary distillation column modeling

The binary distillation column system without time-delay is described as follows [34]:

$$\begin{bmatrix}y_1(s)\\ y_2(s)\end{bmatrix}=\begin{bmatrix}\dfrac{K_{11}}{T_{11}s+1} & \dfrac{K_{12}}{T_{12}s+1}\\ \dfrac{K_{21}}{T_{21}s+1} & \dfrac{K_{22}}{T_{22}s+1}\end{bmatrix}\begin{bmatrix}u_{\rm d1}(s)\\ u_{\rm d2}(s)\end{bmatrix} \tag{32}$$

where y_1 and y_2 are the outputs of the system; $u_{\rm d1}$ and $u_{\rm d2}$ represent the inputs; $K_{11}=12.8$, $K_{12}=-18.9$, $K_{21}=6.6$, $K_{22}=-19.4$, $T_{11}=16.7$, $T_{12}=21$, $T_{21}=10.9$ and $T_{22}=14.4$ are model parameters, where parameter perturbation is ubiquitous.

Carrying out the Laplace transform to (32), we obtain

$$\begin{cases}\ddot{y}_1(t)=f_1+K_{11}u_{\rm d1}(t)/T_{11}T_{12}+K_{12}u_{\rm d2}(t)/T_{11}T_{12}\\ \ddot{y}_2(t)=f_2+K_{21}u_{\rm d1}(t)/T_{21}T_{22}+K_{22}u_{\rm d2}(t)/T_{21}T_{22}\end{cases} \tag{33}$$

where

$$f_1=\frac{K_{11}T_{12}\dot{u}_{11}+K_{12}T_{12}\dot{u}_2-\dot{y}_1(T_{11}+T_{12})-y_1}{T_{11}T_{12}}$$

$$f_2=\frac{K_{21}T_{22}\dot{u}_1+K_{22}T_{21}\dot{u}_2-\dot{y}_1(T_{11}+T_{12})-y_2}{T_{21}T_{22}}$$

Introducing virtual control input $\boldsymbol{u}_{\rm dv}(t)=\boldsymbol{C}_{\rm d}\boldsymbol{u}_{\rm d}(t)$, where $\boldsymbol{u}_{\rm d}(t)=(u_{\rm d1}(t),u_{\rm d2}(t))^{\rm T}$, $\boldsymbol{u}_{\rm dv}(t)=(u_{\rm dv1}(t),u_{\rm dv2}(t))^{\rm T}$, $\boldsymbol{C}_{\rm d}=\begin{bmatrix}K_{11}/T_{11}T_{12} & K_{12}/T_{11}T_{12}\\ K_{21}/T_{21}T_{22} & K_{22}/T_{21}T_{22}\end{bmatrix}$. Substituting it into (33), we obtain

$$\begin{cases}\ddot{y}_1(t)=f_1+u_{\rm dv1}(t)\\ \ddot{y}_2=f_2+u_{\rm dv2}(t)\end{cases}. \tag{34}$$

Design LADRC, NLADRC and SADRC controllers for y_1 channel and y_2 channel respectively in system (34). The parameters of these controllers are shown in Table 1.

Table 1 Parameters of LADRC, NLADRC and SADRC controllers

Controller	y_1 channel	y_2 channel
LADRC [35]	$\xi=1.83$, $w_{\rm o}=13$, $w_c=1.1$, $b_0=10$	$\xi=2.2$, $w_{\rm o}=2$, $w_c=1.68$, $b_0=-14$
NLADRC	$r_1=10$, $h_1=0.45$, $c=0.15$, $\alpha_1=0.5$, $\alpha_2=0.25$, $\delta=0.000\,5$, $\beta_{01}=1$, $\beta_{02}=1.11$, $\beta_{03}=0.173\,6$	$r_1=10$, $h_1=0.45$, $c=0.15$, $\alpha_1=0.5$, $\alpha_2=0.25$, $\delta=0.000\,5$, $\beta_{01}=1$, $\beta_{02}=1.11$, $\beta_{03}=0.173\,6$
SADRC	$\alpha_1=1$, $\alpha_2=0.5$, $\alpha_3=0.25$, $w_c=1.1$, $w_{\rm o}=10$, $w_{\rm oN}=5$, $\delta_s=0.005$, $\delta=0.002$, $b_0=1$, $\beta_{01}=3\,w_{\rm oN}$, $\beta_{02}=3w_{\rm oN}{}^2/5$, $\beta_{03}=w_{\rm oN}{}^3/9$	$\alpha_1=1$, $\alpha_2=0.5$, $\alpha_3=0.25$, $w_c=1.68$, $w_{\rm o}=10$, $w_{\rm o}=5$, $\delta_s=0.005$, $\delta=0.002$, $b_0=1$, $\beta_{01}=3w_{\rm oN}$, $\beta_{02}=3w_{\rm oN}{}^2/5$, $\beta_{03}=w_{\rm oN}{}^3/9$

In Table 1, w_c represents the controller bandwidth of LADRC ; $w_{\rm o}$ and $w_{\rm oN}$ represent the observers of LESO and NLESO, respectively.

In the SADRC based controller for the binary distillation column system, the observer gain $\boldsymbol{L}$ is described as

$$\boldsymbol{L}=\begin{bmatrix}\beta_{01}\cdot\lambda_{01} & 0 & \beta_{02}\cdot\lambda_{02} & 0 & \beta_{03}\cdot\lambda_{03} & 0\\ 0 & \beta_{01}\cdot\lambda_{01} & 0 & \beta_{02}\cdot\lambda_{02} & 0 & \beta_{03}\cdot\lambda_{03}\end{bmatrix}^{\rm T}. \tag{35}$$

According to (15), the value of λ_{0i} (i = 1, 2, 3) is correlated with e. Make curves of λ_{0i} about e, the characteristics are shown in Fig. 2.

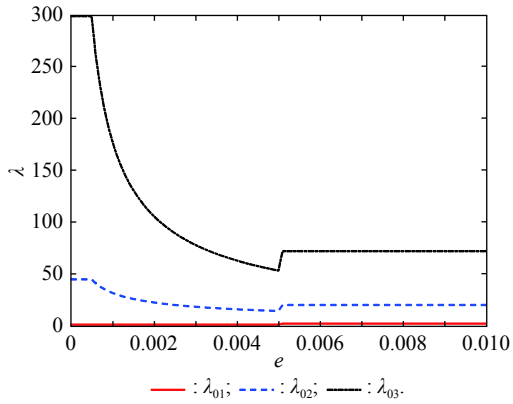

Fig. 2 Curves of λ_{0i} (i = 1,2,3) about e

From Fig. 2, we can conclude that although the value of λ_{0i} (i = 1,2,3) varies with e, it is wobbling within a range. In the entire interval, set 0.002 as the step size, solve Lyapunov functions via Matlab: $(\boldsymbol{A}_0 - \boldsymbol{LQ})^{\mathrm{T}}\boldsymbol{P}_0 + \boldsymbol{P}_0(\boldsymbol{A}_0 - \boldsymbol{LQ}) = \boldsymbol{I}_{6\times6}$, $\boldsymbol{A}_{\mathrm{cl}}^{\mathrm{T}}\boldsymbol{P}_{\mathrm{cl}} + \boldsymbol{P}_{\mathrm{cl}}^{\mathrm{T}}\boldsymbol{A}_{\mathrm{cl}} = \boldsymbol{I}_{10\times10}$. We obtain that there always exist solutions for $\boldsymbol{P}_0$ and $\boldsymbol{P}_{\mathrm{cl}}$. According to Theorem 1 and Theorem 2, the observer error system and the closed-loop system of the SADRC based binary distillation column system is stable independently.

3.1.2 Simulation results

(i) Anti-disturbance simulation

Set the initial value of two channels: $y_1(0) = 0, y_2(0) = 0$, particularly y_1 channel has initial state error, let $z_{11} = 0.2$. Set the target outputs: $y_{d1} = 1, y_{d2} = 1$ at $t = 0$ s, and add the disturbances of the magnitude 0.001 and 0.3, respectively, into the two outputs at t = 25 s. The integrated absolute error (IAE) for each channel is calculated in the whole 50 s. The results are shown in Fig. 3, Fig.4 and Table 2, where IAE = IAE_{y_1} + IAE_{y_2}.

From Fig.3, Fig.4 and Table 2, it can be concluded that: i) All three control methods can realize the decoupling control for the binary distillation column system; ii) LADRC is sensitive to the initial state error, and the performance may deteriorate due to the initial error, while NLADRC and SADRC are insensitive to this; iii) When the disturbance is relative small, the performances of LADRC, NLADRC and SADRC are nearly the same, which means the observer gains of three are all properly chosen and can estimate the disturbance; iv) When the disturbance turns big, the performance of LADRC and SADRC are nearly the same and both superior to NLADRC. Overall, SADRC may be superior to both NLADRC and LADRC in anti-disturbance and can effectively deal with complex circumstances.

In fact, the switching threshold δ_s and the linearity threshold δ can also affect the anti-disturbance performance of the control system, as both of them have influences on the observer gains of SADRC. As a footnote, on the condition that the relationship between the bandwidth of LESO and the one of NLESO remains the same, let δ_s=0.003, 0.005, 0.008, δ=0.000 5, 0.002, respectively, repeat the above anti-disturbance simulation experiments, the performances of the SADRC controllers with different δ_s and δ are shown in Fig.5 and Fig.6, summarized in Table 3 and Table 4.

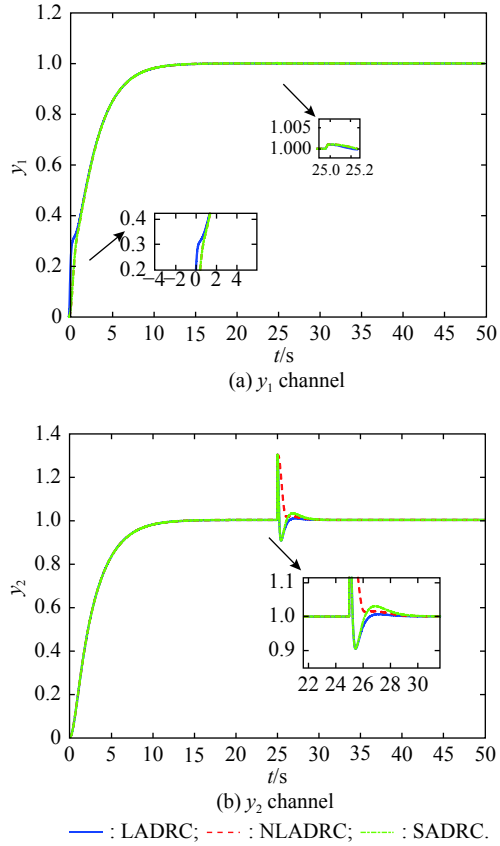

Fig. 3 Tracking performance for the binary distillation column system

From the above results, it can be concluded that: different δ_s and δ have little influence on the performance of the condition that the relationship between the bandwidth of LESO and the one of NLESO is fixed. This is because that δ_s can be determined by theoretical compution [31], when the relationship between the bandwidth of LESO and the one of NLESO is fixed, so is the range of δ_s. The performances with different δ_s of the same order of magnitude are similar. δ aims to suppress high frequency oscillations at zero and though it has influence on the observer gain of NLESO, as $\delta < \delta_s$, when δ_s is fixed, δ in this

paper is too small to have a large effect on the performance of the whole control system.

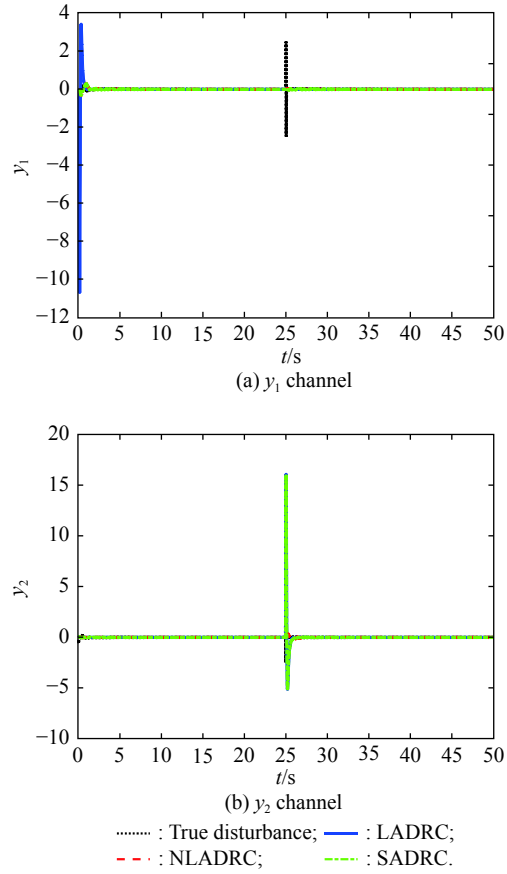

Fig. 4 Observed "total disturbance" for the binary distillation column system

Table 2 Comparison of IAE for the binary distillation column system in anti-disturbance simulation

IAE	LADRC	NLADRC	SADRC
IAE_{y_1}	2.66	2.73	2.73
IAE_{y_2}	3.07	3.16	3.10
IAE	5.73	5.89	5.83

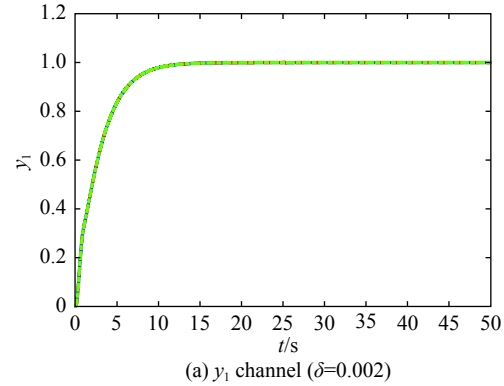

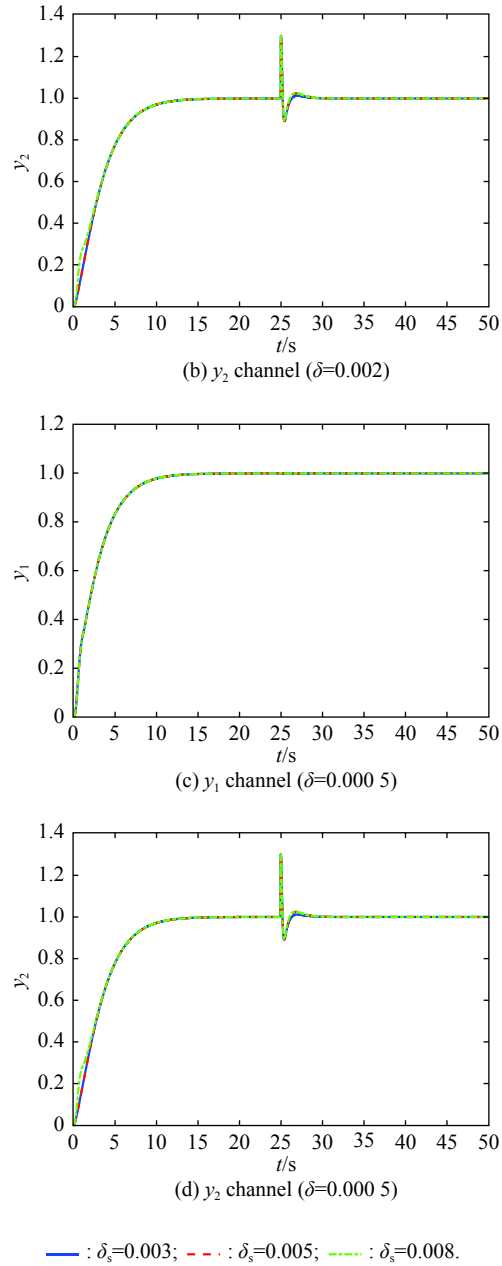

Fig. 5 Tracking performance for the binary distillation column system with a different δ_s and δ

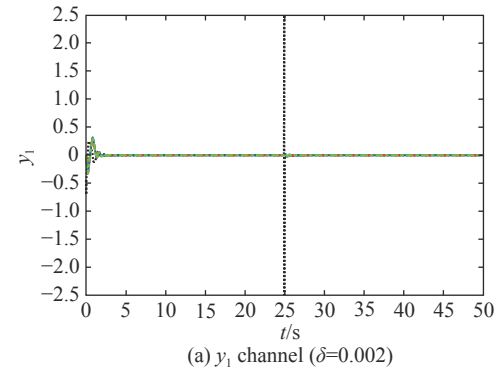

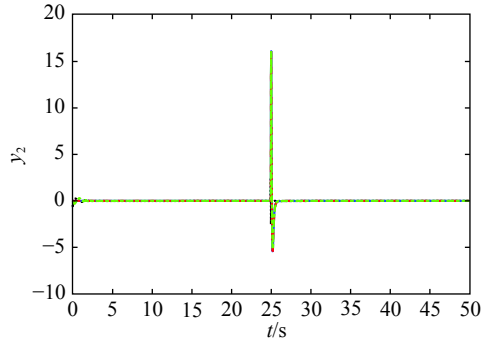

(b) y_2 channel (δ=0.002)

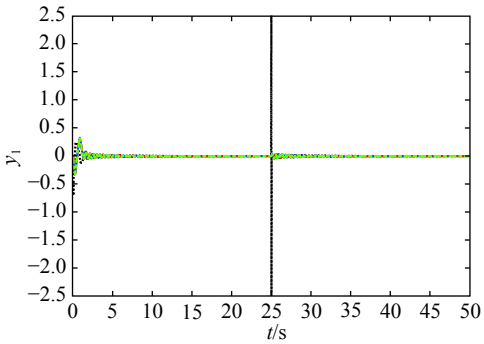

(c) y_1 channel (δ=0.000 5)

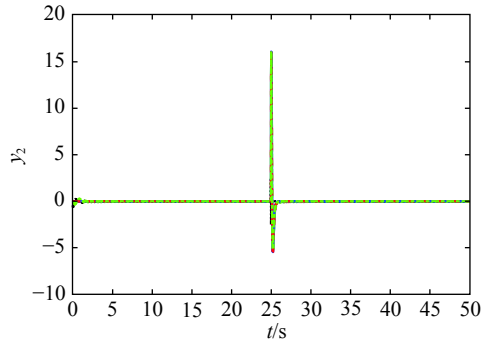

(d) y_2 channel (δ=0.000 5)

: True disturbance; : δ_s=0.003; : δ_s=0.005; : δ_s=0.008.

Fig. 6 Observed "total disturbance" for the binary distillation column system of each channel with a different δ_s and δ

Table 3 Comparison of IAE for the binary distillation column system in anti-disturbance simulation (δ=0.002)

IAE	δ_s=0.003	δ_s=0.005	δ_s=0.008
IAE_{y_1}	2.80	2.73	2.80
IAE_{y_2}	3.09	3.10	3.00
IAE	5.89	5.83	5.80

Table 4 Comparison of IAE for the binary distillation column system in anti-disturbance simulation (δ= 0.000 5)

IAE	δ_s=0.003	δ_s=0.005	δ_s=0.008
IAE_{y_1}	2.80	2.73	2.80
IAE_{y_2}	3.09	3.10	3.00
IAE	5.89	5.83	5.80

(ii) Robustness simulation

Set the initial value of two channels: $y_1(0) = 0, y_2(0) = 0$, and either channel exists state error; set the target outputs: $y_{d1} = 1, y_{d2} = 1$ at $t = 0$ s. Add random perturbation within a range of ±10% to all the parameters in the system (33) before the simulation starts and repeat the simulation by 200 times. Every time the IAE for each channel is calculated in the whole 50 s. The records of overshoot σ and IAE for every experiment are shown in Fig. 7, and summarized in Table 5, where $\sigma = \sigma_{y1} + \sigma_{y2}$; $IAE = IAE_{y1} + IAE_{y2}$.

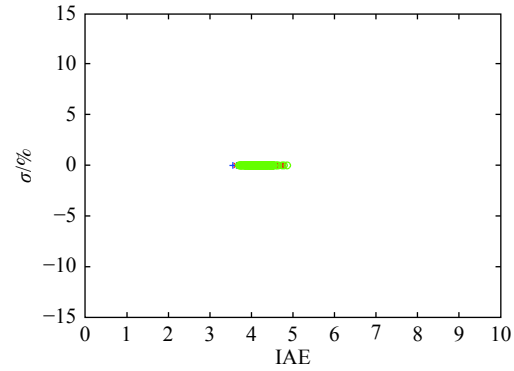

+ : LADRC; × : NLADRC; ○ : SADRC.

Fig. 7 Robustness performance for the binary distillation column system

Table 5 Comparison of IAE for the binary distillation column system in robustness simulation

Overshoot σ and IAE	LADRC	NLADRC	SADRC
σ_{y_1}	0	0	0
σ_{y_2}	0	0	0
σ	0	0	0
IAE_{y_1}	1.60	1.65	1.62
IAE_{y_2}	2.33	2.47	2.42
IAE	3.93	4.12	4.04

From Fig. 7 and Table 5 we can conclude that: i) The intensity of the points reveals that all three control methods have decent robustness; ii) The robustness of LADRC is a little better among all three control methods, and SADRC and NLADRC are nearly the same. That is caused by the small tracking error, which means that NLADRC mainly works in the whole simulation in the SADRC controller, so the performances of the SADRC controller and the NLADRC one are similar, and the observer gain of LADRC is bigger than that of NLADRC, leading to that the tracking error converges to zero more quickly, as a result, the IAE of LADRC is thus smaller.

3.2 Attitude control for 3-DOF Hover

3.2.1 3-DOF Hover model

The attitude model of the 3-DOF Hover system can be

described [36] as

$$\begin{cases} \ddot{\phi} = \dfrac{lK_f(V_r - V_l) + \dot{\theta}\dot{\psi}(J_y - J_z) - K_{afx}\dot{\phi})}{J_x - \dot{\theta}J_{rz}(q_l + q_r - q_b - q_f)/J_x} \\ \ddot{\theta} = \dfrac{lK_f(V_f - V_b) + \dot{\phi}\dot{\psi}(J_z - J_x) - K_{afx}\dot{\theta})}{J_y - \dot{\phi}J_{rz}(q_l + q_r - q_b - q_f)/J_y} \\ \ddot{\psi} = \dfrac{K_M(V_f - V_r + V_b - V_l) - K_{afz}\dot{\psi}}{J_z + \dot{\phi}\dot{\theta}(J_x - J_y)/J_z} \end{cases} \tag{36}$$

where ϕ, θ and ψ represent the pitch angle, roll angle and yaw angle of the system, respectively; l = 0.197 m represents the distance between the propeller motor and the pivot on the axis; $V_i(i = f, b, l, r)$ represent the front motor voltage, the back motor voltage, the left motor voltage and the right motor voltage; K_f = 0.118 8 N/V represents the thrust-force constant; K_M = 0.003 6 N·m/V is the thurst-torque constant; $K_{afx} = K_{afy}$ = 0.008 N·m/rad/s, K_{afz} = 0.009 N·m/rad/s are the drag constants about the x, y, z axes separately; $J_x = J_z$ = 0.055 2 kg·m^2, J_y = 0.11 kg·m^2 represent the moment of inertia about the x, y, z axes respectively.

Introducing virtual control input $U_i(i$ = 1,2,3), taking the coupling interactions among subsystems as "internal disturbance" of the system and considering the external disturbance $w_i(i$ = 1,2,3) of every subsystem, let $\boldsymbol{\eta} = \begin{bmatrix} \phi & \theta & \psi \end{bmatrix}^{\mathrm{T}}$, $\boldsymbol{\omega} = \dot{\boldsymbol{\eta}}$, then the system (36) can be described as

$$\begin{cases} \dot{\boldsymbol{\eta}} = \boldsymbol{\omega} \\ \dot{\boldsymbol{\omega}} = \boldsymbol{U} + \boldsymbol{F}_{\mathrm{dis}} \end{cases} \tag{37}$$

where $\boldsymbol{U} = \begin{bmatrix} U_1 & U_2 & U_3 \end{bmatrix}^{\mathrm{T}} = \boldsymbol{C}_{\mathrm{b}}\boldsymbol{\psi}_{\mathrm{d}}\boldsymbol{V}^{\mathrm{T}}$; $\boldsymbol{V} = \begin{bmatrix} V_f & V_b & V_r & V_l \end{bmatrix}^{\mathrm{T}}$;

$$\boldsymbol{C}_{\mathrm{b}} = \begin{bmatrix} \dfrac{lK_f}{J_x} & 0 & 0 \\ 0 & \dfrac{lK_f}{J_y} & 0 \\ 0 & 0 & \dfrac{K_M}{J_z} \end{bmatrix}; \quad \boldsymbol{\psi}_{\mathrm{d}} = \begin{bmatrix} 0 & 0 & 1 & -1 \\ 1 & -1 & 0 & 0 \\ -1 & -1 & 1 & 1 \end{bmatrix};$$

$\boldsymbol{F}_{\mathrm{dis}}$ represents the "total disturbance", and can be described as

$$\begin{cases} f_1(\cdot) = \dfrac{\dot{\theta}\dot{\psi}(J_y - J_z) - \dot{\theta}J_{rz}(q_l + q_r - q_b - q_f) - K_{afx}\dot{\phi})}{J_x + w_1} \\ f_2(\cdot) = \dfrac{\dot{\phi}\dot{\psi}(J_z - J_x) - \dot{\phi}J_{rz}(q_l + q_r - q_b - q_f) - K_{afy}\dot{\theta}n}{J_y + w_2} \\ f_3(\cdot) = \dfrac{\left[\dot{\phi}\dot{\theta}(J_x - J_y) - K_{afz}\dot{\psi}\right]}{J_z + w_3 n} \end{cases}.$$

Design LADRC, NLADRC and SADRC controllers for ϕ channel, θ channel and ψ channel respectively in system (37). The parameters of these controllers are shown in Table 6.

In the SADRC based controller for 3-DOF Hover system, the observer gain $\boldsymbol{L}$ is described as

$$\boldsymbol{L} = \begin{bmatrix} \beta_{\phi 01}\cdot\lambda_{\phi 01} & 0 & 0 & \beta_{\phi 02}\cdot\lambda_{\phi 02} & 0 & 0 & \beta_{\phi 03}\cdot\lambda_{\phi 03} & 0 & 0 \\ 0 & \beta_{\theta 01}\cdot\lambda_{\theta 01} & 0 & 0 & \beta_{\theta 02}\cdot\lambda_{\theta 02} & 0 & 0 & \beta_{\theta 03}\cdot\lambda_{\theta 03} & 0 \\ 0 & 0 & \beta_{\psi 01}\cdot\lambda_{\psi 01} & 0 & 0 & \beta_{\psi 02}\cdot\lambda_{\psi 02} & 0 & 0 & \beta_{\psi 03}\cdot\lambda_{\psi 03} \end{bmatrix}^{\mathrm{T}}. \tag{38}$$

Table 6 Parameters of LADRC, NLADRC, SADRC controllers

Controller	ϕ channel	θ channel	ψ channel
LADRC [36]	w_o = 28, w_c = 2.8, b_0 = 0.424	w_o = 30, w_c = 3, b_0 = 0.424	w_o = 30, w_c = 3.2, b_0 = 0.213
NLADRC [37]	ESO: α_1 = 0.75, α_2 = 0.5, α_3 = 0.25, β_{01} = 30, β_{02} = 300, β_{03} = 1 000, b_0 = 0.9, δ = 0.006, NLESF: δ = 3, α_1 = 0. 5, α_2 = 0.05, β_1 = 150, β_2 = 120	ESO: α_1 = 0.75, α_2 = 0.5, α_3 = 0.25, β_{01} = 30, β_{02} = 300, β_{03} = 1 000, b_0 = 0.9, δ = 0.006, NLESF: δ = 3, α_1 = 0. 5, α_2 = 0.05, β_1 = 150, β_2 = 120	ESO: α_1 = 0.75, α_2 = 0.5, α_3 = 0.25, b_0 = 0.06, δ = 0.004, h = 0.001 5, β_{01} = 30, β_{02} = 300, β_{03} = 1 000, NLESF: δ = 1, α_1 = 0. 5, α_2 = 0.05, β_1 = 300, β_2 = 180
SADRC	α_1 = 1, α_2 = 0.5, α_3 = 0.25, w_c = 2.8, w_o = 30, w_{oN} = 15, δ_s = 0.005, b_0 = 0.424, δ = 0.002, $\beta_{01} = 3w_{oN}$, $\beta_{02} = 3w_{oN}^2/5$, $\beta_{03} = w_{oN}^3/9$	α_1 = 1, α_2 = 0.5, α_3 = 0.25, w_c = 3, w_o = 30, w_{oN} = 15, δ_s = 0.005, b_0 = 0.424, δ = 0.002, $\beta_{01} = 3w_{oN}$, $\beta_{02} = 3w_{oN}^2/5$, $\beta_{03} = w_{oN}^3/9$	α_1 = 1, α_2 = 0.5, α_3 = 0.25, w_c = 3.2, w_o = 30, w_{oN} = 15, δ_s = 0.005, b_0 = 0.033, δ = 0.002, $\beta_{01} = 3w_{oN}$, $\beta_{02} = 3w_{oN}^2/5$, $\beta_{03} = w_{oN}^3/9$

Within the entire intervals of λ_{01}, λ_{02} and λ_{03}, set 0.002 as the step size, solve Lyapunov functions via Matlab; $(\boldsymbol{A}_0 - \boldsymbol{LQ})^{\mathrm{T}}\boldsymbol{P}_0 + \boldsymbol{P}_0(\boldsymbol{A}_0 - \boldsymbol{LQ}) = \boldsymbol{I}_{9\times 9}$, $\boldsymbol{A}_{\mathrm{cl}}{}^{\mathrm{T}}\boldsymbol{P}_{\mathrm{cl}} + \boldsymbol{P}_{\mathrm{cl}}{}^{\mathrm{T}}\boldsymbol{A}_{\mathrm{cl}} = \boldsymbol{I}_{15\times 15}$, and we obtain that there always exist solutions for $\boldsymbol{P}_0$ and $\boldsymbol{P}_{\mathrm{cl}}$. According to Theorem 1 and Theorem 2, the observer error system and the closed-loop system of the SAD-

RC based 3-DOF Hover system is stable separately.

3.2.2 Simulation results

(i) Anti-disturbance simulation

Set the initial value of three channels: $\phi(0) = 0°$, $\theta(0) = 0°$, $\psi(0) = 0°$, and ϕ channel and θ channel have initial state error separately, let $z_{1\phi} = 0.04°$, $z_{1\theta} = 0.4°$. Set the target outputs: $\phi_d = 3°$, $\theta_d = 3°$, $\psi_d = 3°$ at $t = 0$ s. Add the disturbances of the magnitude 0.04°, 0.6°, and 1° into the three outputs at $t = 25$ s for 3 s, respectively. The results are shown in Fig. 8, Fig. 9 and Table 7.

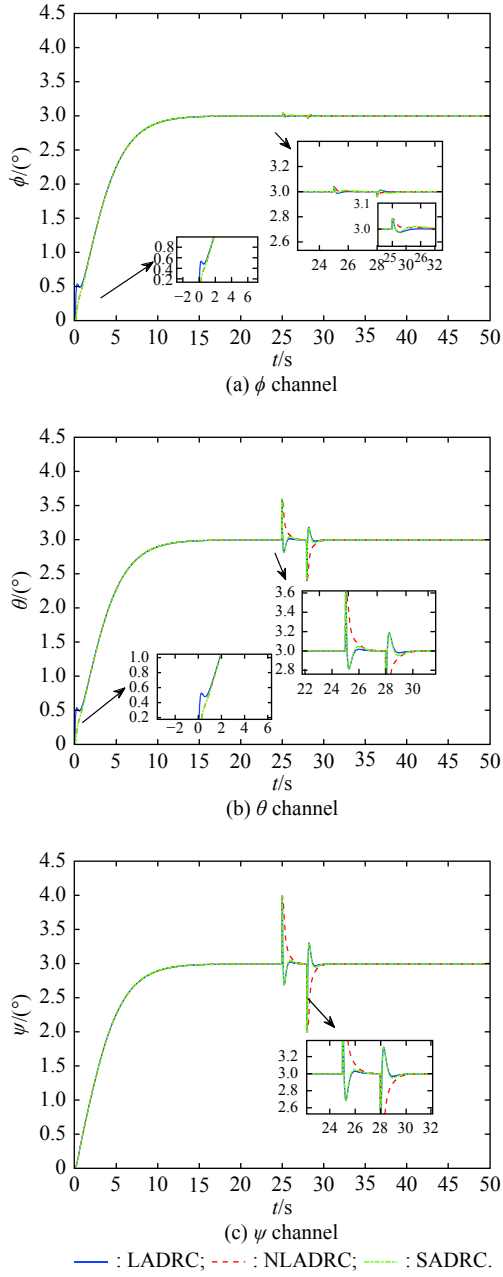

Fig. 8 Tracking performance for the 3-DOF Hover system

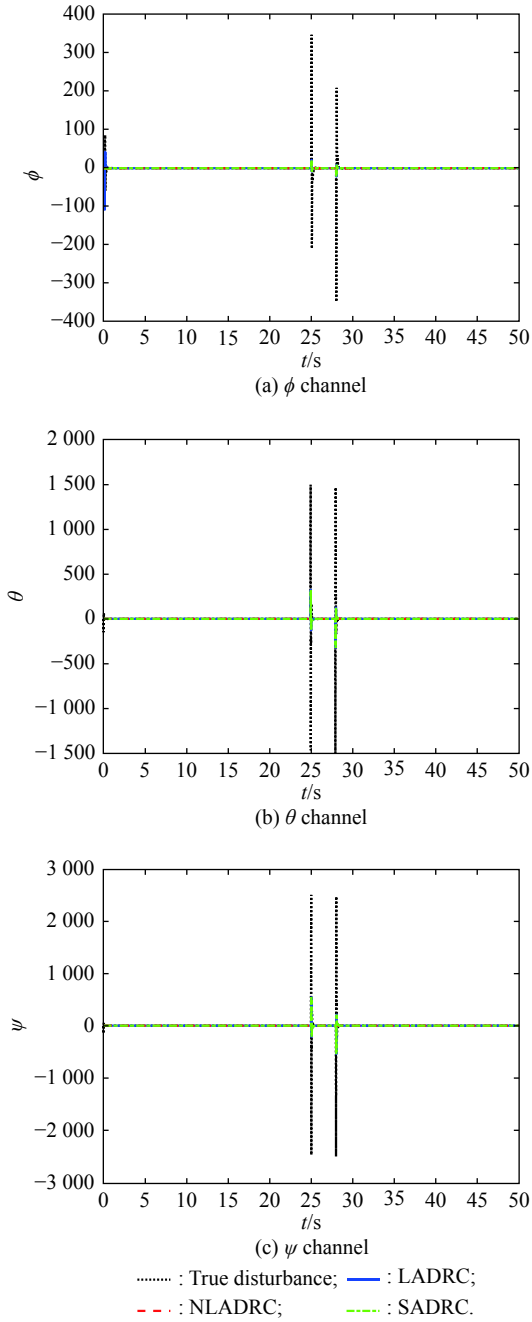

Fig. 9 Observed "total disturbance" for the 3-DOF Hover system

Table 7 Comparison of IAE for the 3-DOF Hover system in anti-disturbance simulation

IAE	LADRC	NLADRC	SADRC
IAE_ϕ	10.54	10.71	10.68
IAE_θ	10.61	11.13	10.84
IAE_ψ	13.31	13.93	13.30
IAE	34.46	35.77	34.82

The performances of SADRC controllers with different δ_s and δ also have been taken into consideration in this part. On the condition that the relationship between

the bandwidth of LESO and the one of NLESO remains the same, let δ_s=0.003, 0.005, 0.008, δ=0.000 5, 0.002, respectively, repeat the above anti-disturbance simulation experiments in Subsection 3.2.2, the performances of the SADRC controllers with different δ_s and δ are shown in Fig. 10 and Fig. 11 and summarized in Table 8 and Table 9.

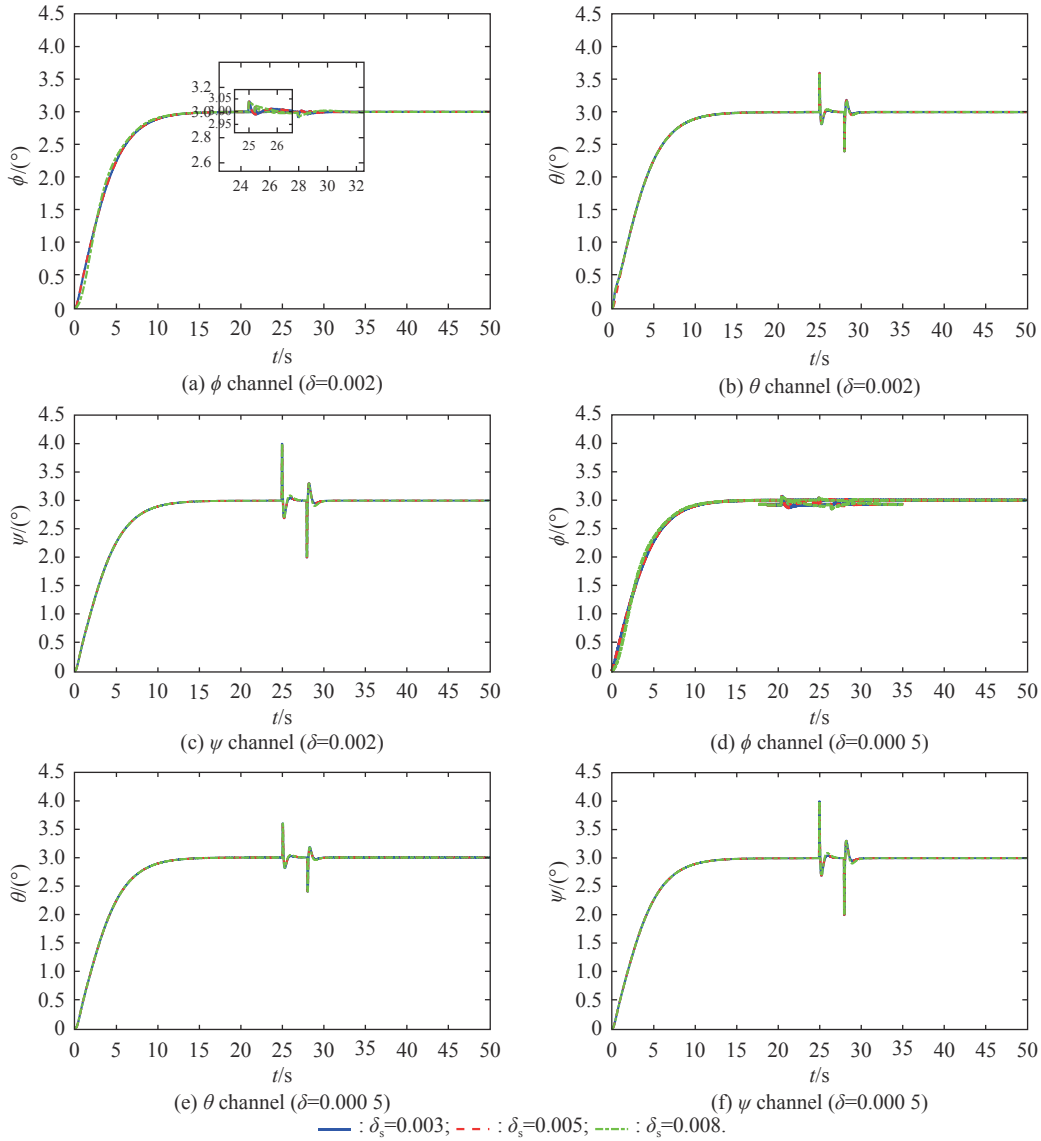

Fig. 10 Tracking performance for the 3-DOF Hover system with a different δ_s and δ

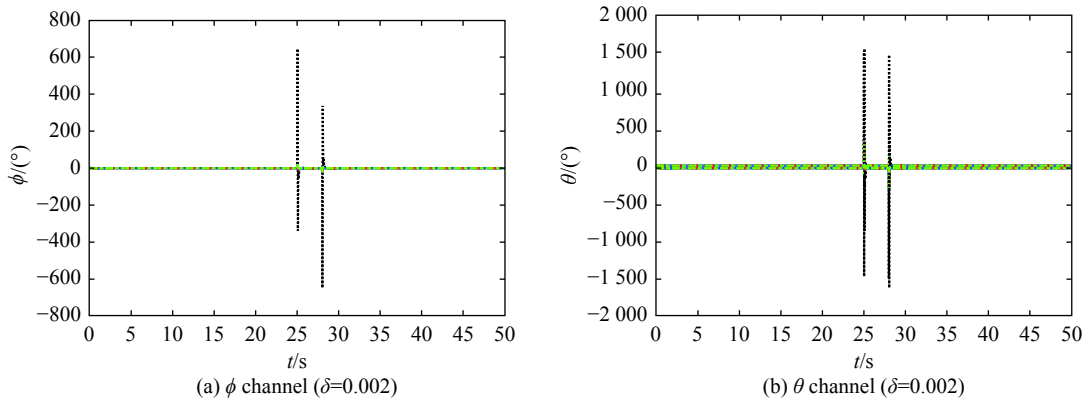

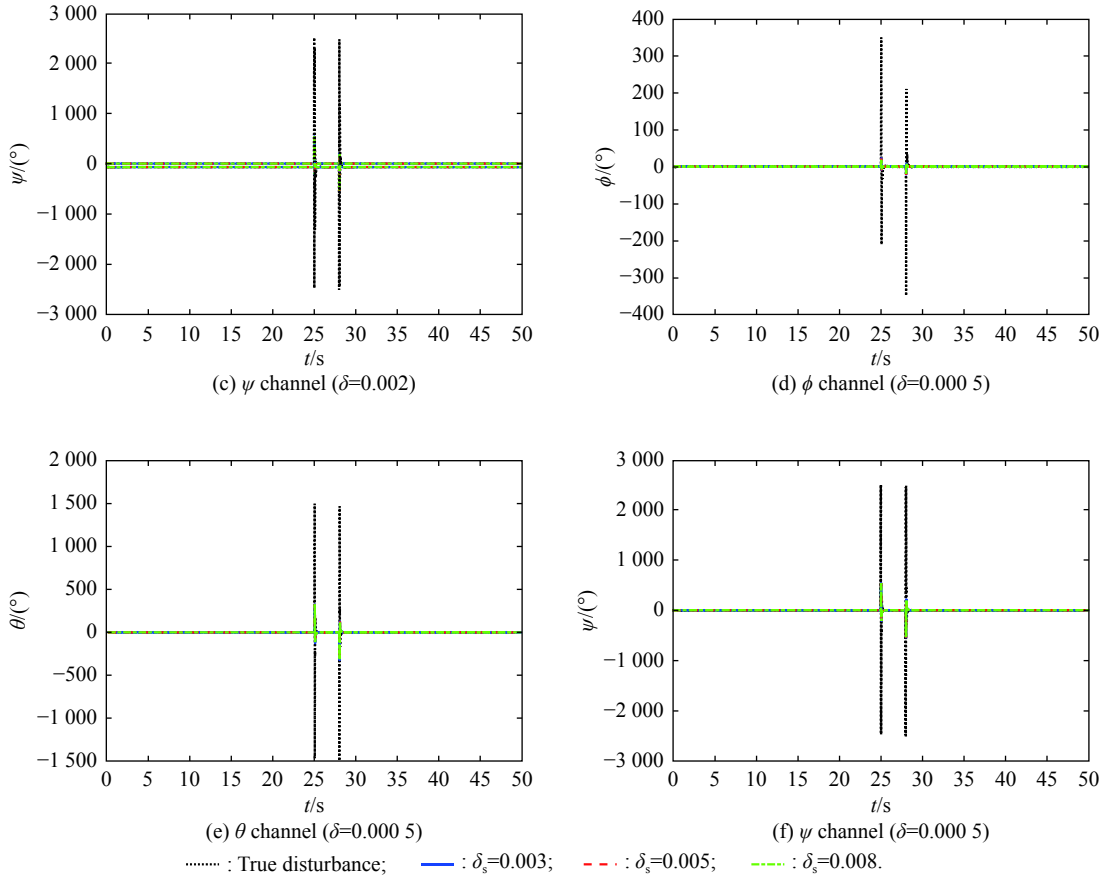

Fig. 11 Observed "total disturbance" for the 3-DOF Hover system of each channel with a different δ_s and δ

Table 8 Comparison of IAE for the 3-DOF Hover system in anti-disturbance simulation (δ= 0.002)

IAE	δ_s=0.003	δ_s=0.005	δ_s=0.008
IAE_ϕ	10.68	10.68	10.70
IAE_θ	10.81	10.84	10.82
IAE_ψ	13.30	13.30	13.25
IAE	34.79	34.82	34.77

Table 9 Comparison of IAE for the 3-DOF Hover system in anti-disturbance simulation (δ= 0.000 5)

IAE	δ_s=0.003	δ_s=0.005	δ_s=0.008
IAE_ϕ	10.68	10.69	10.70
IAE_θ	10.82	10.85	10.83
IAE_ψ	13.31	13.31	13.29
IAE	34.81	34.85	34.82

The results once again prove that different δ_s and δ will influence the performance, but the influences are not obvious under the current experimental condition.

(ii) Robustness simulation

Set the initial value of three channels: $\phi(0) = 0°$, $\theta(0) = 0°$, $\psi(0) = 0°$, and none channel exists has error. Set the target outputs: $\phi_d = 3°$, $\theta_d = 3°$, $\psi_d = 3°$ at $t = 0$ s. Add random perturbation within a range of ±10% to all the parameters in the system (37) before the simulation starts and repeat the simulation by 200 times. Every time the IAE for each channel is calculated in the whole 50 s. The records of overshoot σ and IAE for every experiment are shown in Fig. 12, and summarized in Table 10, where $\sigma = \sigma_\phi + \sigma_\theta + \sigma_\psi$; $IAE = IAE_\phi + IAE_\theta + IAE_\psi$.

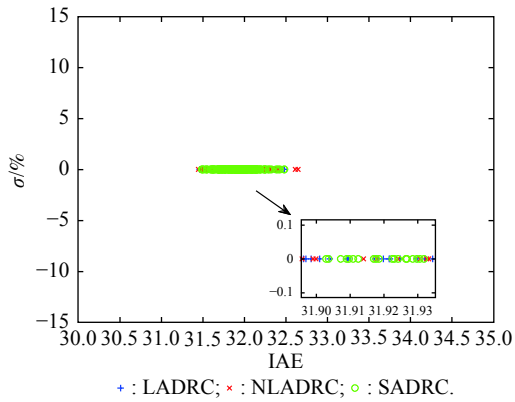

Fig. 12 Robustness performance for the 3-DOF Hover system

Table 10 Comparison of IAE for the 3-DOF Hover system

Overshoot σ and IAE	LADRC	NLADRC	SADRC
σ_ϕ	0	0	0
σ_θ	0	0	0
σ_ψ	0	0	0
σ	0	0	0
IAE_ϕ	10.60	10.85	10.73
IAE_θ	10.62	10.81	10.71
IAE_ψ	12.42	13.86	13.36
IAE	33.64	35.52	34.80

From the above results, we can conclude that: i) The proved decoupling control approach can also be applied to the systems that the number of inputs and outputs is not equal; ii) The performance of LADRC is sensitive to the initial state error, when the initial state error is relatively big, its performance may deteriorate due to the "peaking phenomenon", while the initial state error has little influence on the performance of NLADRC and SADRC; iii) The NLADRC is more suitable to deal with relative small disturbance while LADRC is suitable to deal with the relative big one. In general, SADRC may be superior to both NLADRC and LADRC in terms of the anti-disturbance and robustness in occasions where the amplitude of the disturbance is unsure or unstable, as it combines the advantages of both LADRC and NLADRC.

4. Conclusions

In this paper, the SADRC based decoupling control approach is proposed for a class of MIMO continuous systems, which can be applied to systems with equal or unequal number of inputs or outputs. Stability of the closed-loop system is also proved. The stability analysis method is based on the Lyapunov function and does not require an accurate model, only the number of subsystems, the order of the subsystem and the parameters of controllers are needed. It is convenient for engineering applications and can provide references for parameter tuning. Two cases also verify that the SADRC may be superior to both NLADRC and LADRC in the anti-disturbance and robustness in some occasions as it combines the advantages of both systems. However, the proposed stability analysis method is achieved by means of computer calculation and is not rigorous enough in theory to some extent. Other approaches will be characterized to give strict theoretical proofs for stability analysis in the near future.

References

[1] HAN J Q, WANG W. Nonlinear tracking-differentiator. Journal of System and Mathematical Science, 1994, 14(3): 177–183. (in Chinese)

[2] HAN J Q, YUAN L L. The discrete form of tracking-differentiator. Journal of System and Mathematical Science, 1999, 19(3): 268–273. (in Chinese)

[3] HAN J Q. Nonlinear state error feedback control law — NLSEF. Control and Decision, 1995, 10(3): 221–226. (in Chinese)

[4] HAN J Q. The "extended state observer" of a class of uncertain systems. Control and Decision, 1995, 10(1): 85–88. (in Chinese)

[5] HAN J Q. Auto-disturbance rejection controller and it's applications. Control and Decision, 1998, 13(1): 19–23. (in Chinese)

[6] HAN J Q. Linear and nonlinear in feedback systems. Control and Decision, 1988, 3(2): 27–32. (in Chinese)

[7] HAN J Q. Control theory, is it a model analysis approach or a direct control approach. Journal of System and Mathematical Science, 1989, 9(4): 328–335. (in Chinese)

[8] ZHAO Z L, GUO B Z. On convergence of nonlinear active disturbance rejection control for a class of nonlinear systems. Journal of Dynamical and Control Systems, 2016, 22(2): 385–412.

[9] GUO B Z, ZHAO Z L. On convergence of the nonlinear active disturbance rejection control for MIMO systems. Journal on Control and Optimization, 2013, 51(2): 1727–1757.

[10] ZHAO Z L, GUO B Z. Active disturbance rejection control approach to stabilization of lower triangular systems with uncertainty. International Journal of Robust and Nonlinear Control, 2015, 26(11): 2314–2337.

[11] WU D, CHEN K. Frequency-domain analysis of nonlinear active disturbance rejection control via the describing function method. IEEE Trans. on Industrial Electronics, 2013, 60(9): 3906–3914.

[12] WU D, CHEN K. Limit cycle analysis of active disturbance rejection control system with two nonlinearities. ISA Transactions, 2014, 53(4): 947–954.

[13] LI J, QI X H, XIA Y Q, et al. Frequency domain stability analysis of nonlinear active disturbance rejection control system. ISA Transactions, 2015, 56(5): 188–195.

[14] LI J, XIA Y Q, QI X H, et al. Absolute stability analysis of nonlinear active disturbance rejection control for single-input-single-output systems via the circle criterion method. IET Control Theory & Applications, 2015, 9(15): 2320–2329.

[15] QI X H, LI J, XIA Y Q, et al. On the robust stability of active disturbance rejection control for SISO systems. Circuits, Systems, and Signal Processing, 2017, 35(1): 65–81.

[16] LI J, XIA Y Q, QI X H. Robust absolute stability analysis for interval nonlinear active disturbance rejection based control system. ISA Transactions, 2017, 69: 122–130.

[17] WAN H. Stability and application for active-disturbance-rejection-controller. Beijing: Academy of Mathematics and Systems Science, 2001. (in Chinese)

[18] LI J, QI X H, XIA Y Q, et al. On asymptotic stability for nonlinear ADRC based control system with application to the ball-beam problem. Proc. of American Control Conference, 2016: 4725–4730.

[19] GAO Z Q. Scaling and bandwidth—parameterization based controller tuning. Proc. of American Control Conference, 2003: 4989–4996.

[20] LI R H, CAO J H, LI T S. Active disturbance rejection control design and parameters configuration for ship steering with wave disturbance. Control Theory & Applications, 2018, 35(11): 1601–1609. (in Chinese)

[21] YOO D, STEPHEN S T, GAO Z. On convergence of the linear ex-tended state observer. Proc. of the IEEE International Symposium on Intelligent Control, 2006: 1645–1650.

[22] YANG X, HUANG Y. Capability of extended state observer for estimating uncertainties. Proc. of American Control Con-

ference, 2009: 3700 – 3705.
[23] SHAO L W, LIAO X Z, XIA Y Q, et al. Stability analysis and synthesis of third order extended state observer. Information and Control, 2008, 37(2): 135 – 139.
[24] YOO D, YAU S T, GAO Z. Optimal fast tracking observer band-width of the linear extended state observer. International Journal of Control, 2007, 80(1): 102–111.
[25] HUANG Y, WANG J, SHI D. On convergence of extended state observers for discrete-time nonlinear systems. Proc. of the 34th Chinese Control Conference, 2015: 551 – 556.
[26] ZHENG Q, GAO L Q, GAO Z. On stability analysis of active disturbance rejection control for nonlinear time-varying plants with unknown dynamics. Proc. of the 46th IEEE Conference on Decision and Control, 2007: 3501 – 3506.
[27] CHEN Z Q, SUN M W, YANG R G. On stability analysis of linear disturbance rejection control. Acta Automatica Sinica, 2013, 39(5): 574–580. (in Chinese)
[28] XUE W, HUANG Y. Comparison of the DOB based control, a special kind of PID control and ADRC. Proc. of American Control Conference, 2011: 4373 – 4379.
[29] XUE W, HUANG Y. The active disturbance rejection control for a class of MIMO blocklower-triangular system. Proc. of the 31st Chinese Control Conference, 2011: 6362 – 6367.
[30] XUE W, HUANG Y. On performance analysis of ADRC for non-linear uncertain systems with unknown dynamics and discontinuous disturbances. Proc. of the 32nd Chinese Control Conference, 2013: 465 – 470.
[31] LI J, XIA Y Q, QI X, et al. On the necessity, scheme and basis of the linear-nonlinear switching in active disturbance rejection control. IEEE Trans. on Industrial Electronics, 2017, 64(2): 1425–1435.
[32] LI J, QI X H, XIA Y Q, et al. On linear/nonlinear active disturbance rejection control. Acta Automatica Sinica, 2016, 42(2): 202–212. (in Chinese)
[33] MOKHTARI R M, BRAHAM A C, CHERKI B. Extended state observer based control for coaxial-rotor UAV. ISA Transactions, 2015, 11(24): 1–14.
[34] SU S X, YANG H Z. Active-disturbance-rejection dynamic nonlinear decoupling control for a class of multivariable systems. CIESC Journal, 2010, 61(8): 1949–1954.
[35] LIU Q, LI D, TIAN W. Design of multi-loop ADRC controllers based on the effective open-loop transfer function method. Proc. of the 33rd Chinese Control Conference, 2014: 3649 – 3654.
[36] LIU M, JI Y H, LI J F, et al. Active disturbance rejection attitude control for quadrotor aircraft. Computer Simulation, 2016, 33(3): 711–75.
[37] LI Y, CHEN Z Q, SUN M W, et al. Attitude control for quadrotor helicopter based on discrete-time active disturbance rejection control. Control Theory & Applications, 2015, 32(11): 1470–1477. (in Chinese)

Biographies

WAN Hui was born in 1991. She received her B.E. and M.E. degrees from the Department of Unmanned Aerial Vehicle Engineering, the former Mechanical Engineering College, Shijiazhuang, China, in 2014 and 2016, respectively. She is currently working towards her Ph.D. degree in Army Engineering University. Her research interests include theory and application of active disturbance rejection control and flight control of unmanned aerial vehicle.
E-mail: huiwan_0425@163.com

QI Xiaohui was born in1963. She received her B.E., M.E. and Ph.D. degrees from Nanjing University of Science and Technology, Nanjing, China, in 1983, 1988, 2010, respectively. She is currently a professor at the Department of Unmanned Aerial Vehicle Engineering, Army Engineering University of PLA. Her research interests include flight control theory and application for unmanned aerial vehicle, and adaptive control.
E-mail: qi-xh@163.com

LI Jie was born in 1987. He received his B.E., M.E. and Ph.D. degrees from the Department of Unmanned Aerial Vehicle Engineering, the former Mechanical Engineering College, Shijiazhuang, China, in 2010, 2012, 2016, respectively. Currently, he is working towards his Ph.D. degree in Army Engineering University. His research interests include theory and application of active disturbance rejection control, particularly fully exerting advantages of the nonlinear mechanism.
E-mail: lijienewlife1234@163.com